



CHORUS

This is the accepted manuscript made available via CHORUS. The article has been published as:

Retrieval of material parameters for uniaxial metamaterials

Georgia T. Papadakis, Pochi Yeh, and Harry A. Atwater

Phys. Rev. B **91**, 155406 — Published 7 April 2015

DOI: [10.1103/PhysRevB.91.155406](https://doi.org/10.1103/PhysRevB.91.155406)

Retrieval of material parameters for uniaxial metamaterials

Georgia T. Papadakis^{1,†}, Pochi Yeh² and Harry A. Atwater¹

¹ *Thomas J. Watson Laboratories of Applied Physics, California Institute of Technology, California 91125, USA*

² *Department of Electrical and Computer Engineering, University of California, Santa Barbara, California 93106, USA*

†Corresponding author e-mail: gpapadak@caltech.edu

Abstract

We present a general method for retrieving the effective tensorial permittivity of uniaxially anisotropic metamaterials. By relaxing the usually-imposed constraint of assuming non-magnetic metal/dielectric metamaterials, we also retrieve the effective permeability tensor and show that multilayer hyperbolic metamaterials exhibit a strong and broadband diamagnetic response in the visible regime. The method provides the means for designing magnetically anisotropic metamaterials for studying magnetic topological transitions in the visible regime. We obtain orientation-independent effective material parameters, which are distinguishable from mere wave parameters. We analytically validate this method for Ag/SiO₂ planar metamaterials with a varying number of layers and filling fractions, and compare to the results from effective medium theory and Bloch theory.

Keywords

Effective medium theory, transfer matrix, uniaxial anisotropy, hyperbolic metamaterials (HMM), isofrequency contour, density of optical states

I. Introduction

Today's nanofabrication techniques enable us to build artificial composite media, also called metamaterials (MM), with sub-wavelength unit cells, usually termed meta-atoms. MMs can be engineered to have extraordinary optical properties that cannot be found in nature; examples include negative refractive index^{1,2}, reversed Doppler effect², epsilon near zero^{3,4} and super-resolution⁵ (see Ref. [6] and references therein). The meta-atom arrangement, which is periodic in most cases, is a crucial parameter for controlling light propagation in the MM and thus its optical response. Specifically, uniaxial MMs that have permittivities with opposite sign along different coordinate directions, also called hyperbolic metamaterials⁷ (HMMs), have attracted considerable attention because a) they can support negative refraction^{7,8}, hyper-lensing⁹ and a high density of optical states^{10,11} among other phenomena and b) they are straightforward to fabricate, since they can be realized in a stack of metal-dielectric multilayers with sub-wavelength thicknesses or with metallic nanowires in a dielectric host. HMMs are also the most popular candidates for studying topological transitions in MMs^{11,12}. These factors motivate the present work to develop parameter retrieval methods for both electric and magnetic parameters applicable to HMMs.

Provided that the wavelength of light is much larger than the unit cell of the MM, the collective response of a MM can be approximated by that of a homogeneous medium. An effective permittivity and permeability can then be introduced¹³⁻¹⁶. However, most retrieval methods reported so far consider only

normal incidence^{14, 15, 17}. In a previous report¹³, a new retrieval procedure for angle-dependent effective parameters was introduced. As these authors noted in their work, the retrieved parameters are then “mere *wave* parameters rather than global *material* parameters”. Thus, no direct information regarding the anisotropy of the MM (i.e. its effective birefringence or dichroism), a key feature for HMMs, is directly obtained. Additionally, wave parameters cannot be directly measured experimentally, nor do they represent constitutive parameters of the material. To be useful effective material parameters, the retrieved parameters ought to be independent of the polarization and the angle of incidence, independent of the wave-vector (local) and of the total MM thickness in the long wavelength limit. Studies on the validity of effective material parameters applied to fishnet type MMs and to split-ring resonator MM structures have been presented in [18, 19] respectively.

In this paper, we show that, upon homogenization of a MM, using for example methods like those in [13], the utilization of the general dispersion equations for uniaxially anisotropic materials enables us to retrieve global effective permittivities and permeabilities along all coordinate directions, that satisfy the effective material parameter criteria mentioned above. It is important to note that, unlike the approaches taken by previous researchers^{7, 10, 11, 20-25}, we do not assume, a priori, a unity magnetic permeability along all symmetry directions. Instead, we use the general dispersion relations for magnetic uniaxial slabs to retrieve an effective permeability tensor, in addition to the effective permittivity tensor. Until now, metal/dielectric HMMs have been assumed to be non-magnetic^{7, 10, 11, 20-25} at optical frequencies. We show by contrast that they can exhibit strong diamagnetic behavior. We show that the retrieval of the complex constitutive parameters is analytical and not subject to any numerical fitting process^{26, 27}. We systematically compare our solution to the inverse problem of parameter retrieval with results of solution to the forward problem of calculation of transmission and reflection calculations with known optical parameters of the constituent materials of the MMs and we obtain excellent agreement between inverse and forward calculations for all angles of incidence. Since HMMs are usually realized with periodic alterations of the refractive index in a uniaxial geometry, we apply our method to periodic HMMs with finite total thickness and compare our results to the generalized method of Bloch theorem (See [28], Ch. 6), valid in the infinite thickness limit.

The effective response of a MM is often approximated with an effective medium theory. The two most widely used effective medium theories in the MMs field are the generalized effective medium approximation²⁹ and the Bruggeman³⁰ approximation. Both of them are based on field averaging over the unit-cell scale. The generalized effective medium approximation is the most commonly used method for approximating an effective permittivity tensor for HMMs^{7, 10, 11, 25, 29, 31-33}. However, it is only valid for low filling fractions and it fails to predict the diamagnetic characteristics of planar metal/dielectric metamaterials that we emphasize in this paper. We compare our analysis to the effective medium approximation to highlight the importance of a) the total number of layers in planar metal/dielectric HMMs b) and of the relative filling fraction of metal and dielectric and c) also the importance of taking into account the magnetic character of HMMs on their effective response. We show that these factors, which are not considered in the effective medium picture, significantly limit the regime where the effective medium theory is appropriate as a model for physically realizable MMs.

This paper is structured as follows. In part II we provide a short description of the previous work done in Ref. [13], we introduce the additional correction for uniaxial anisotropy and present our methodology. In part III, we demonstrate the application of our method to a homogeneous finite slab of Ag, as a special case of a uniaxial material with equal elements of the diagonal permittivity and

permeability tensors, and to Ag/SiO₂ multilayer MMs with varying number of layers. We compare our calculations to the effective medium approximation. We also illustrate the diamagnetic response of planar HMMs. In part IV we calculate the isofrequency contours for a magnetic uniaxial MM slab to highlight the importance of an accurate retrieval method for HMMs. In part V we perform a parameter sweep over the thickness of the individual metal/dielectric layers and filling fractions and compare our results to the effective medium approximation.

II. Method

a. Homogenization

We perform homogenization using the general approach of [13]. Thus, once the complex reflection and transmission coefficients of a slab with finite thickness and unknown optical parameters are calculated for any angle of incidence and for transverse electric (TE) or transverse magnetic (TM) polarization, a scalar complex permittivity and permeability can be analytically calculated. An effective wave-vector for wave propagation inside the unknown MM is also obtained, under the assumption that the slab is homogeneous. However, if no further assumption is made regarding the anisotropy of the slab, as indicated in [13], the retrieved parameters, denoted as ϵ_{TE} , μ_{TE} , ϵ_{TM} and μ_{TM} are *wave* parameters and not fundamental *material* parameters. They exhibit strong angle dependence even for isotropic materials, but this is also true for fishnet structures (See Ref.13) and for the planar metal-dielectric MMs studied here, as we prove in the next subsection. Thus, the parameters ϵ_{TE} , μ_{TE} , ϵ_{TM} and μ_{TM} , which are presented in the supplemental material, are given for completeness, but they are not essential for the determination of the MM material parameters. Relative to the notation adopted in [13], we interchange ϵ_{TM} and μ_{TM} , due to the correspondence of the electric and magnetic field between TE and TM polarization in homogeneous media. The modal effective refractive indices for the TE and TM waves respectively are defined as: $n_{TE} = \sqrt{\epsilon_{TE}\mu_{TE}}$ and $n_{TM} = \sqrt{\epsilon_{TM}\mu_{TM}}$. It is the scope of this paper to emphasize that, after such a homogenization is performed, it is possible and rather simple to retrieve electric permittivity and magnetic permeability tensor elements that are independent of the angle of incidence and can fully characterize a HMM.

b. Dispersion equations for a magnetic uniaxial crystal

Now we determine the dispersion for a magnetic uniaxial material by introducing the constraint that the slab with unknown parameters is uniaxial and its optical axis coincides with the direction of normal incidence (denoted as the z axis in the Fig. 1a). As noted in the introduction, the two most popular uniaxial MM motifs are multilayer thin film stacks and arrays of nano-wires embedded in a host material.

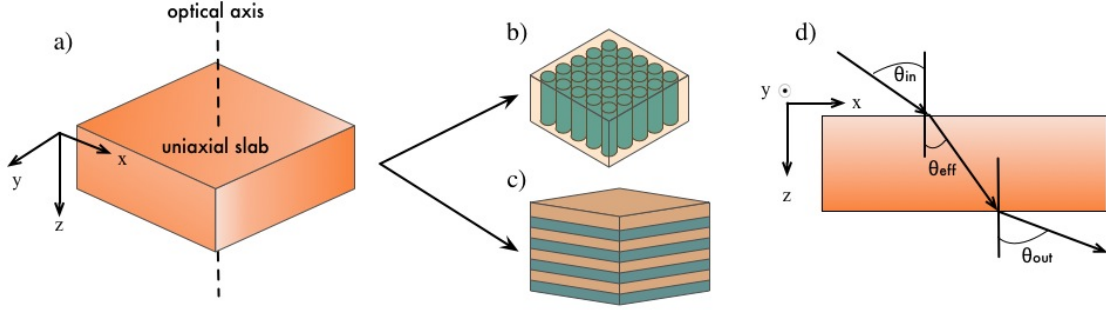


Fig. 1: a) three dimensional representation of the unknown uniaxial slab that can be, among others, b) a nanowire array or c) a multilayer stack. d) projection of a) onto the xz plane, convention for the angle of incidence

Assuming a monochromatic plane wave $\mathbf{E}(\mathbf{r}, t) = \mathbf{E}_0 e^{i(kr - \omega t)}$ propagating in a general bianisotropic medium with tensorial permittivity $\vec{\epsilon}$ and permeability $\vec{\mu}$, Helmholtz's equation²⁸ yields:

$$k \times \vec{\mu}^{-1} (k \times E) + \omega^2 \vec{\epsilon} E = 0 \quad (1)$$

For a uniaxial slab, since the optical axis is aligned to the z axis, the permittivity and permeability tensors are diagonal with $\vec{\epsilon} = \text{diag}(\epsilon_{xx}, \epsilon_{yy}, \epsilon_{zz}) = \text{diag}(\epsilon_o, \epsilon_o, \epsilon_e)$ and $\vec{\mu} = \text{diag}(\mu_{xx}, \mu_{yy}, \mu_{zz}) = \text{diag}(\mu_o, \mu_o, \mu_e)$

where we replaced $\epsilon_{xx} = \epsilon_{yy}$ with ϵ_o , the ordinary permittivity of a uniaxial slab and ϵ_{zz} with ϵ_e , the extraordinary permittivity of the slab. Similar replacements are performed for the permeability tensor elements μ_o and μ_e . (Here we refer to ϵ_o and μ_o as the ordinary parameters in order to be consistent with the literature of non-magnetic uniaxial materials²⁸, and likewise for the extraordinary parameters). Carrying out the algebra of Eq. (1), the dispersion equations for magnetic uniaxial crystals are:

$$\text{Magnetically extraordinary wave: } \frac{k_x^2 + k_y^2}{\epsilon_o \mu_e} + \frac{k_z^2}{\epsilon_o \mu_o} = k_o^2 \quad (2a)$$

$$\text{Electrically extraordinary wave: } \frac{k_x^2 + k_y^2}{\epsilon_e \mu_o} + \frac{k_z^2}{\epsilon_o \mu_o} = k_o^2 \quad (2b)$$

where $k_o = \omega / c$. These equations indicate that, for a magnetic uniaxial slab, the dispersion surface consists of two ellipsoids of revolution. The parameters $\epsilon_o, \mu_o, \epsilon_e, \mu_e$ are fundamental, angle and thickness independent, *material* parameters. We emphasize here that a HMM can be designed not only by requiring permittivities of opposite signs along different axes for the electrically extraordinary wave but also by requiring permeabilities of opposite signs along different axes for the magnetically extraordinary wave, as recently demonstrated in the microwave regime¹².

For propagation in the xz plane, i.e. for $k_y = 0$, the magnetically extraordinary wave corresponds to electric field parallel to the y axis (TE polarization) while the electrically extraordinary wave corresponds to magnetic field parallel to the y axis (TM polarization). Here k_x is the in-plane wave vector which is conserved above, inside and below the slab. For TE polarization,

$k_x = k_0 \sin \theta_{in} = n_{TE} k_0 \sin \theta_{eff}$ and $k_z = n_{TE} k_0 \cos \theta_{eff}$, similarly for TM polarization. k_z is the normal component of the wave vector in the slab. For MM slabs k_z stands for the effective wave vector usually retrieved via homogenization in terms of the complex reflection and transmission coefficients, the polarization and the incident angle θ_{in} ¹³. Thus, Eq. (2a) and (2b) can be associated with the wave parameters for TE and TM polarization, ϵ_{TE} , μ_{TE} , ϵ_{TM} and μ_{TM} :

$$\text{Magnetically extraordinary wave: } \frac{1}{\epsilon_{TE}(\theta_{in})\mu_{TE}(\theta_{in})} = \frac{\sin^2 \theta_{eff}}{\epsilon_o \mu_e} + \frac{\cos^2 \theta_{eff}}{\epsilon_o \mu_o} \quad (3a)$$

$$\text{Electrically extraordinary wave: } \frac{1}{\epsilon_{TM}(\theta_{in})\mu_{TM}(\theta_{in})} = \frac{\sin^2 \theta_{eff}}{\epsilon_e \mu_o} + \frac{\cos^2 \theta_{eff}}{\epsilon_o \mu_o} \quad (3b)$$

where θ_{eff} is the refraction angle into the slab (See Fig. 1d). Since the denominators of the right hand side of Eqs. (3a) and (3b) ought be angle-independent, the wave parameters are angle-dependent (See [13], [18] and supplemental material Figs. 12-15).

c. Retrieval of material parameters ϵ_o , μ_o and ϵ_e , μ_e

For normal incidence, $k_z = n_{TE}(\theta_{in} = 0)k_0 = n_{TM}(\theta_{in} = 0)k_0$ and from the equations above we obtain: $n_{TE}^2(\theta_{in} = 0) = n_{TM}^2(\theta_{in} = 0) = \epsilon_o \mu_o$. Thus, $\epsilon_o = \epsilon_{TE}(\theta_{in} = 0) = \epsilon_{TM}(\theta_{in} = 0)$ and $\mu_o = \mu_{TE}(\theta_{in} = 0) = \mu_{TM}(\theta_{in} = 0)$. This is expected since at normal incidence the two polarizations are degenerate. Thus, the application of the wave parameter retrieval method [13] for normal incidence yields the ordinary parameters of any uniaxial slab in the geometry illustrated in Fig.1.

By having already retrieved the ordinary parameters ϵ_o , μ_o from wave parameter retrieval at normal incidence, wave parameter retrieval at an oblique incident angle for TE polarization, together with Eq. (2a), is sufficient for determination of the effective extraordinary permeability μ_e . Specifically, for a non-zero in-plane wave vector $k_x(\theta_{in}) = n_c \frac{\omega}{c} \sin \theta_{in}$ where n_c is the refractive index of the cladding, and for the retrieved through the homogenization $k_{zTE}(\theta_{in})$, we obtain the extraordinary permeability by solving Eq. (2a) for μ_e . Similarly, to retrieve the effective extraordinary permittivity ϵ_e , application of the wave parameter retrieval at an oblique incident angle for TM polarization, together with Eq. (2b) suffice. In this case, the out of plane wave vector must correspond to TM polarization: $k_{zTM}(\theta_{in})$. The equations for calculation of $k_{zTE/TM}$ are given in Appendix A. For any oblique angle of incidence, application of Eqs. (2a) and (2b) yields angle-independent parameters, as we prove below for planar HMMs with varying number of layers.

To summarize, our approach to the retrieval problem for inhomogeneous uniaxial MMs is based on replacing the actual system by a homogeneous uniaxial effective medium characterized by ϵ_o , μ_o , ϵ_e and μ_e , which is the so-called inverse scattering problem. The first step in our approach is to obtain the physical system's complex reflection and transmission coefficients for the two polarizations, which is

defined here as the forward problem. When homogenization is valid and in the long wavelength regime, only two incident angles suffice for determining ϵ_o , μ_o , ϵ_e and μ_e : for normal incidence scattering, wave parameter retrieval yields ϵ_o and μ_o . Wave parameter retrieval at one oblique incident angle is sufficient to yield the effective wave vector k_z for both polarizations, which, together with the use of the dispersion Eqs. (2a) and (2b) yields the extraordinary parameters ϵ_e and μ_e . The method is repeated as a consistency check for different incident angles. If convergence of the extraordinary parameters for different incident angles is achieved, local material parameters can be assigned and the retrieval is successful, as we demonstrate in the next section for planar HMMs. The degree of angle independence of the extraordinary parameters can be viewed as a metric of the locality of the considered MM^{18, 20}. For a perfectly local medium, all angles of incidence must yield identical extraordinary parameters. The diagram shown below summarizes the method.

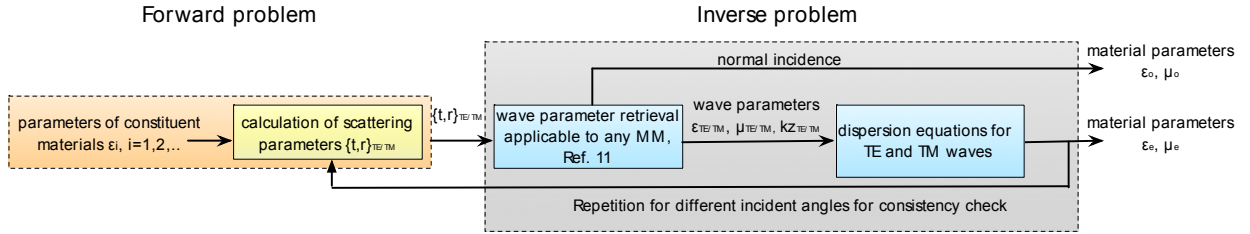


Fig. 2: diagram of the retrieval steps

III. Application to a slab of Ag and to planar Ag/SiO₂ HMMs

We give here results for material parameter retrieval applied to a 20nm thick Ag slab, which is viewed as a special case of a uniaxial material with $\epsilon_o = \epsilon_e$ and $\mu_o = \mu_e = 1$, and to a planar MM consisting of 7 alternating layers of Ag and SiO₂, with thicknesses 20nm each. A five pole Drude-Lorentz (DL) model was used for the dielectric function of Ag ϵ_{Ag_DL} ³⁴. The Sellmeier equation was used for the refractive index of SiO₂³⁴. Using the transfer matrix method²⁸ for layered media, we calculate the complex reflection and transmission coefficients for angles of incidence $0^\circ - 90^\circ$ for TE and TM polarization.

a. Retrieval of material parameters $\epsilon_o, \mu_o, \epsilon_e$ and μ_e

Upon application of the steps presented in Sections II a-c, we show below the retrieved material parameters for the 20nm Ag slab, in Fig. 3a and b and for the 7 layers of Ag and SiO₂ in Fig. 3c and d.

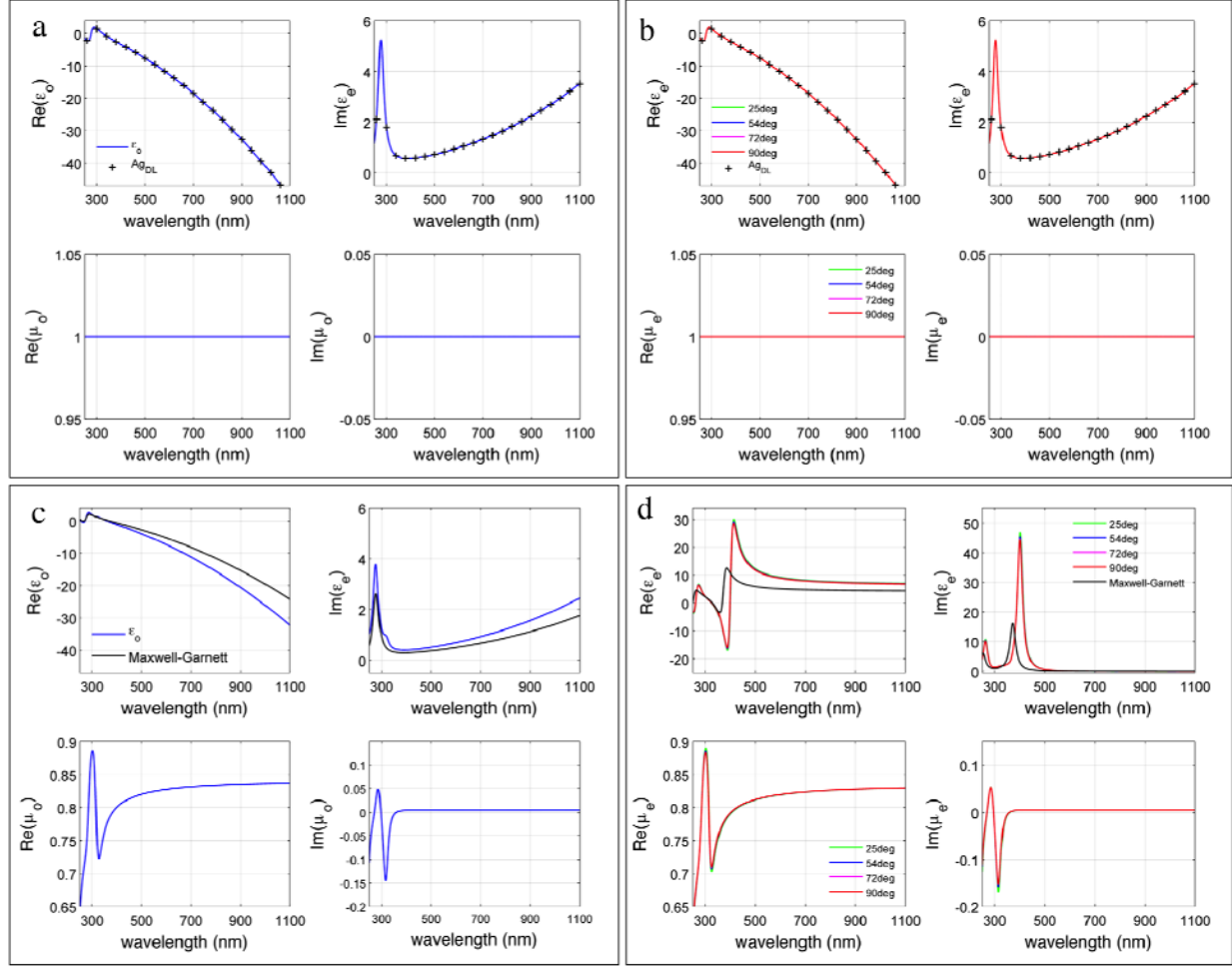


Fig. 3: ϵ_o , μ_o for a) a slab of Ag and c) a MM consisting of 7 alternating layers of Ag and SiO_2 . ϵ_e , μ_e for different incident angles for a) a single layer of Ag, and d) the 7 layer MM

For the single slab of Ag, the ordinary permittivity ϵ_o (Fig. 3a), calculated at normal incidence, trivially converges to the 5-pole Drude-Lorentz model of Ag: ϵ_{Ag_DL} . Similarly, the ordinary permeability μ_o in Fig. 3a, is exactly unity, as expected for a non-magnetic slab. It is remarkable that the extraordinary parameters ϵ_e and μ_e calculated at different considered angles of incidence ranging from $25^\circ - 90^\circ$ all converge to the same curves, as shown in Fig. 3b. Similarly to ϵ_o , ϵ_e converges to ϵ_{Ag_DL} for all the considered angles of incidence, while $\mu_e = 1 + 0i$ for all angles. To conclude, for a single slab of Ag the application of the retrieval trivially yields $\epsilon_o = \epsilon_e = \epsilon_{Ag_DL}$ and $\mu_o = \mu_e = 1 + 0i$ for all angles of incidence $0^\circ - 90^\circ$, yielding a consistency check for the model for the case of an isotropic non-magnetic slab.

Concerning Fig. 3c, for the 7 layer MM, the predominantly metallic response is expected in the xz plane where $Re(\epsilon_o) < 0$, since the charge carriers of the metallic layers are free to move in this plane.

However, \mathcal{E}_o is red-shifted with respect to \mathcal{E}_{Ag_DL} , which originates from the insertion of the SiO₂ layers between adjacent Ag layers that results in a less polarizable (meta) material. As seen in Fig. 3c, the exact results from our calculations for \mathcal{E}_o also differ considerably from the generalized effective medium results, shown in black. The disagreement is an effect of the finite total thickness of the 7 layer MM and it is discussed further in the following subsection. Regarding the ordinary permeability μ_o , contrary to a single Ag slab, where μ_o is unity, a 7 layer planar MM is strongly diamagnetic as shown in Fig. 3c.

From Fig. 3d, one can see by inspection the negligible angular variation of both \mathcal{E}_e and μ_e for a 7 layer MM. These parameters converge to the same curves for all the considered angles of incidence. Thus, their ‘‘intrinsic’’ nature as *material* parameters is now apparent. They exhibit almost no spatial dispersion and, thus, they are local. Previous work on non-locality (see Ref.20) has shown that, using Bloch theory for infinite periodic metal/dielectric MMs, one obtains stronger non-locality effects. By contrast, we show here that merely removing the usually imposed constraint of unity magnetic permeability and taking the effect of finite total thickness into account suffice for completely suppressing the non-locality of the effective parameter \mathcal{E}_e .

The Lorentzian-shaped $Im(\mathcal{E}_e)$ and its Kramers-Kronig counterpart $Re(\mathcal{E}_e)$ are also common features in uniaxial crystals existing in nature like calcite at mid-infrared wavelengths²². The disagreement between the calculated \mathcal{E}_e and the effective medium prediction is also an effect of the finite total thickness of the considered MM discussed below. Importantly, we find that the real parts of μ_o and μ_e are non-unity. This issue is discussed further in what follows. We note that in Fig. 3c and 3d, for wavelengths smaller than 350nm, the imaginary parts of μ_o and μ_e are negative, but this is not of any concern since causality is not violated as justified in Appendix B.

b. Effect of the number of layers- Comparison to Effective Medium Theory and diamagnetism

In the effective medium limit, the tensorial permittivity for infinite planar periodic HMMs^{7, 10, 11, 25, 29, 31-33} contains ordinary and extraordinary permittivity elements, which are respectively $\mathcal{E}_o = f\mathcal{E}_m + (1-f)\mathcal{E}_d$ and $\mathcal{E}_e^{-1} = f\mathcal{E}_m^{-1} + (1-f)\mathcal{E}_d^{-1}$, where \mathcal{E}_m is the metal permittivity and \mathcal{E}_d is the dielectric permittivity and f is the filling fraction of the metal in the unit cell. Figure 4 summarizes the results of our calculations for \mathcal{E}_o and \mathcal{E}_e for Ag/SiO₂ MMs with varying number of layers ranging from 3 to 27 layers and we compare to effective medium theory.

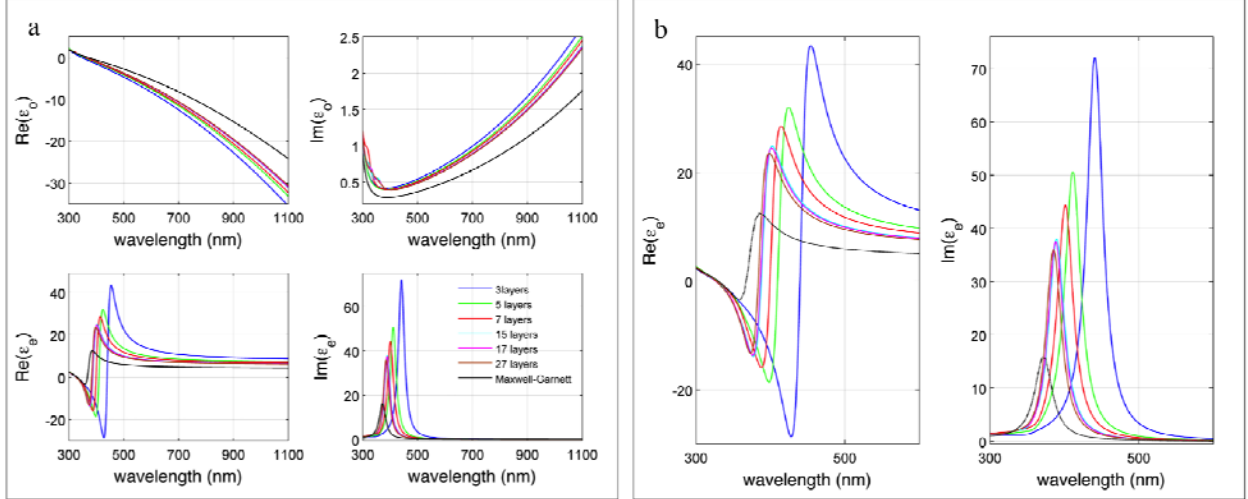


Fig. 4: a) ϵ_o and ϵ_e for planar Ag/SiO₂ MMs with varying number of layers and comparison to the effective medium approximation, b) same results for ϵ_e near resonance

As the number of Ag/SiO₂ layers increases, the calculated permittivities approach the effective medium approximation, which is expected since an asymptotically large number of layers corresponds to an infinite medium²⁹. However, even at 27 layers neither ϵ_o nor ϵ_e converge completely to the effective medium theory results. This deviation deserves special attention because the wavelengths at which the permittivities along different coordinate directions cross zero are fundamental for the prediction of the wavelengths at which topological transitions occur in HMMs^{11, 12}. From Fig. 4b, the wavelength at which the real part of ϵ_e crosses zero, which corresponds to the center of the Lorentzian-shaped $Im(\epsilon_e)$, blueshifts as the number of layers increases. This wavelength is important for the distinction between the spectral regions at which the MM exhibits a hyperbolic or an elliptical dispersion, giving rise to very different optical response. Importantly, there is also a clear discrepancy between the amplitude of the Lorentzian resonance in $Re(\epsilon_e)$ in the effective medium limit and our calculations. This affects the shape of isofrequency contours of the MM as shown in Section IV.

In the effective medium limit, HMMs are usually considered to be non-magnetic along all coordinate directions. That this is an erroneous assumption is clearly demonstrated in the Fig. 5, which gives the ordinary and extraordinary permeability for Ag/SiO₂ planar MMs with varying number of layers. We note that the difference between μ_o and μ_e is of the order of 10^{-3} for these MMs, so they can be considered as magnetically isotropic with $\mu_o \approx \mu_e$.

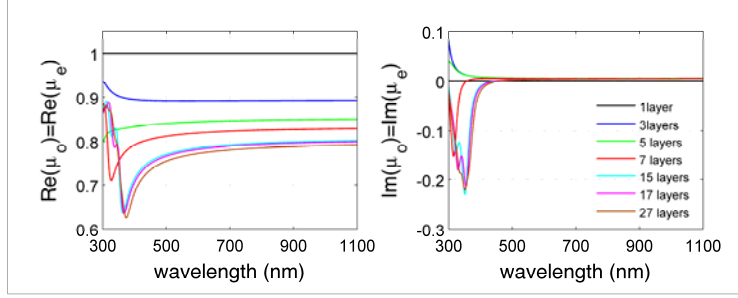


Fig. 5: a) μ_o and μ_e for planar Ag/SiO₂ MMs with varying number of layers

We find from Fig. 5 that with an increasing number of Ag/SiO₂ layers, HMMs become more diamagnetic with μ_o and μ_e being as low as 0.65. The most diamagnetic material existing in nature is bismuth with a permeability of 0.999834. Thus, multilayer HMMs exhibit a strong diamagnetic response, which, according to electromagnetic boundary conditions, arises from induced surface currents at the Ag/SiO₂ interfaces, created by the tangential component of the applied magnetic field. It is expected that an increasing number of layers results to a stronger diamagnetic response because this is accompanied with an increase of the number of metal-dielectric interfaces where surface currents are induced. According to Lenz's law, the induced currents must create a magnetic response that opposes the applied magnetic field; thus they create a diamagnetic response which translates to a permeability smaller than unity. The imaginary parts of the ordinary and extraordinary permeability are negative in the short wavelength regime for multilayers with more than 5 layers, but this does not violate any physical law, as justified in Appendix B.

IV. Comparison of Isofrequency Surfaces from Retrieved Material Parameters and Effective Medium Model

The effective k-space or isofrequency contours are of crucial importance for describing the response of MMs to single-frequency excitation. Using Eq. (2a) and (2b) we show in Fig. 6 the isofrequency contours of the 7 layer Ag/SiO₂ HMM, given the values of ϵ_o , ϵ_e , μ_o and μ_e obtained in the preceding sections. In the effective medium approximation, the permeability in different axes is usually assumed to be unity, and in this limit Eq. (2a) and (2b) become: $(k_x^2 + k_z^2) = \epsilon_o k_o^2$ and $(k_x^2 / \epsilon_e + k_z^2 / \epsilon_o) = k_o^2$ respectively, which are commonly used to describe HMMs^{7, 10, 11, 25, 29, 31-33}. We are only taking account of the real parts of the denominators of k_x and k_z as their imaginary parts can be directly translated to a complex frequency instead of a complex k-space³⁵. We also include the isofrequency curves as determined using Bloch theorem for layered periodic media²⁸, which is valid when periodic boundary conditions are imposed.

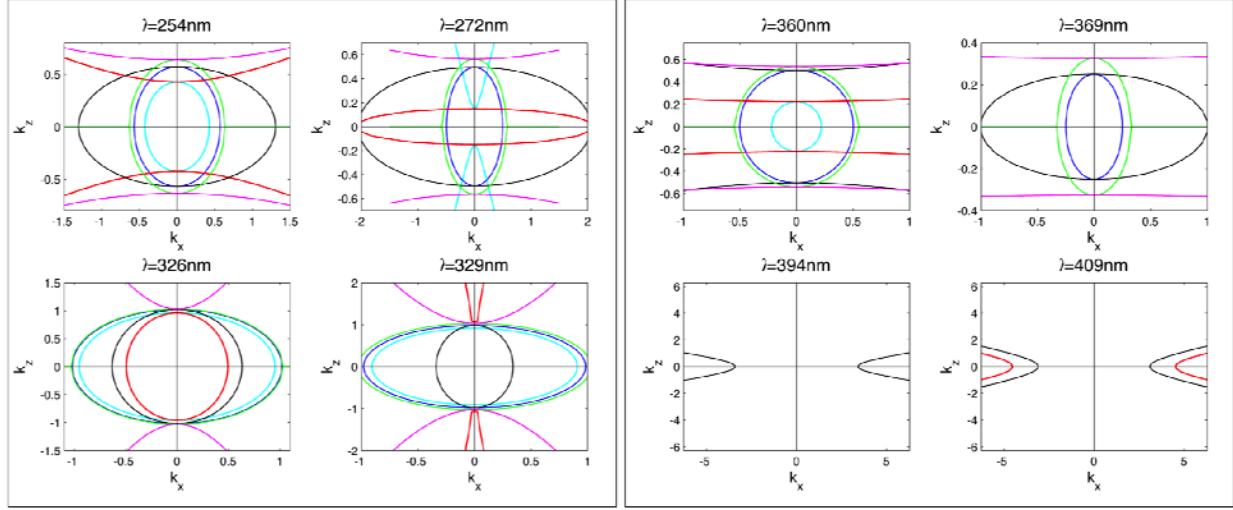


Fig. 6: Effective k-space for 7 layer Ag/SiO₂ HMM and comparison to generalized effective medium theory. Results of the retrieval are shown with light blue color for TE polarization and with red for TM polarization. The generalized effective medium approximation is shown with dark blue for TE polarization and black for TM polarization. Bloch theory results are shown with green for TE polarization and magenta for TM polarization

We note that effective medium theory and our retrieval give rise to isofrequency contours with different shapes, as it can be seen comparing the dark blue curves to the light blue ones (TE polarization) in Fig. 6, and the red curves to the black curves (TM polarization) respectively. Not only does the surface area enclosed by the isofrequency contour (which is proportional to the total number of available optical states¹⁰) differ between our calculations and the generalized effective medium approximation, we find that for TM polarization at some wavelengths, even the nature of the dispersion is predicted to be different. For example, at 254nm and at 329nm, the effective medium approximation predicts elliptical dispersion (black curves), whereas our calculations predict hyperbolic dispersion (red curves). It is also worth highlighting that, within the 3nm interval between 326nm and 329nm, our model predicts a change in the dispersion surface from elliptical to hyperbolic, as one can note by comparing the isofrequency contours for those wavelengths. The wavelengths at which the dispersion surface changes shape correspond to the wavelengths for which topological transitions can occur.

For TE polarization the isofrequency contours are almost circular, revealing the very weak magnetic anisotropy of the planar HMMs (See light blue lines). In the lossless limit, when $\epsilon_o\mu_o$ and $\epsilon_o\mu_e$ are negative, Eq. (2a) is only satisfied for imaginary wave vectors, which translates to exponential decay of the TE wave inside the MM. This situation is similar to the situation in which a homogeneous metal becomes a perfect reflector for frequencies below the plasma frequency. According to our calculations, this effectively metallic response for the TE wave occurs for wavelengths above 362nm, whereas in the effective medium limit this transition occurs at 372nm. This is the reason for the absence of light blue curves in the figures above for the wavelengths 369nm, 394nm and 409nm, indicating a zero photonic density of states in the lossless limit according to our model. Similarly, the absence of dark blue curves for the wavelengths 394nm and 409nm indicates a zero density of photonic states in this MM according to the effective medium approximation. Here it is also worth noting the agreement between Bloch theory results and the effective medium results for TE polarization: the dark blue contours and the green contours almost overlap for all considered wavelengths since both approaches consider infinite stacks.

The strong disagreement between the exact results and the Bloch theory results is another indication that the effects of finite total thickness of physically realizable HMMs are significant on the shape of the isofrequency contours and, as a consequence, on the total number of supported optical states.

A similar situation as the one described for the TE polarization occurs for the TM wave. According to our calculations (Fig. 3c,d), there exists a region where both $\epsilon_o\mu_o$ and $\epsilon_e\mu_o$ are negative: from 362nm, where the product $\epsilon_o\mu_o$ crosses zero, up to 401nm, where the product $\epsilon_e\mu_o$ returns to positive values. Thus, for these wavelengths, there exists an effective omnidirectional bandgap for the TM wave in the MM. This is why no red isofrequency contours are present in Fig. 6 for the wavelengths of 369nm and 394nm, indicating the absence of photon states. Importantly, for wavelengths smaller than 362nm, the retrieval predicts that this MM supports a region of hyperbolic dispersion type I ($\epsilon_e\mu_o < 0$ and $\epsilon_o\mu_o > 0$), while for wavelengths larger than 401nm, the hyperbolic dispersion is of type II ($\epsilon_e\mu_o > 0$ and $\epsilon_o\mu_o < 0$). On the other hand, the effective medium approximation does not predict neither the hyperbolic type I region (see for example Fig. 6 for 329nm) nor the effective bandgap, since the black curves are present for 369nm and 394nm in Fig. 6, indicating the existence of photon states for those wavelengths in the effective medium picture.

Bloch theory results, shown with magenta for TM polarization, deviate from both the effective medium picture (black contours) and the exact results (red contours). The former is a consequence of the fact that, in the effective medium limit, the surface charges on metal/dielectric interfaces are not taken into account²⁹. This is unphysical since the TM wave carries an electric field component normal to the interfaces that induces charges at metal/dielectric interfaces. By contrast, Bloch theory results are obtained using the transfer matrix approach, in which the electric field discontinuity normal to the interfaces due to induced charges is taken into account²⁸. The discrepancy between Bloch theory and our calculations indicate that the finite total thickness of the HMM and the type of layer (metal or dielectric) that terminates the structure significantly affect the isofrequency surface. However we note that the exact results do approach the Bloch theory results as the number of layers increases.

In order to investigate on the existence of this omnidirectional bandgap for the TM wave, we take into account the complex nature of Eq. (2b). We calculate the effective normal wave vector in the 7 layer Ag/SiO₂ MM in terms of the retrieved complex parameters ϵ_o , μ_o and ϵ_e , as a function of the normalized in-plane wave vector k_x/k_o and the wavelength. As shown in Fig. 7, in the region where the real parts of $\epsilon_o\mu_o$ and $\epsilon_e\mu_o$ are negative ranging from 362-401nm, the real part of the normalized normal wave vector is negligible compared to the imaginary part, validating our argument that this corresponds to a true omnidirectional bandgap that is not predicted by the generalized effective medium theory.

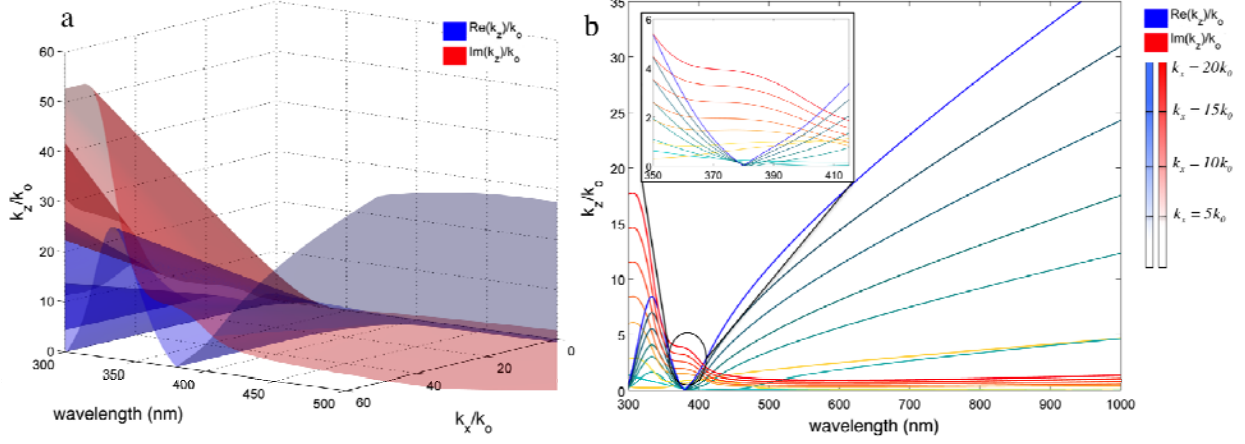


Fig.7: a) Real-blue and imaginary-red parts of effective normalized k_z as a function of the in plane wave vector and the wavelength. b) Projected version of a): darker blue curves correspond to real part of normalized k_z for increasing k_x , darker red curves correspond to imaginary part of normalized k_z for increasing k_x

V. Filling fraction and thickness effects- Comparison to Effective Medium Theory

In this section, we investigate the effects of individual metal and dielectric layer thickness on the effective parameters, and compare to effective medium theory. We fix the total thickness of the HMM to be 140nm and we consider 7 alternating layers of Ag and SiO₂. We let the metallic filling fraction vary between the values of $f=0.25, 0.3, 0.4, 0.5, 0.7$ and 0.9 which correspond respectively to Ag layers thickness of 11nm, 13nm, 16nm, 20nm, 26nm and 32nm. The corresponding thicknesses for SiO₂ are 32nm, 30nm, 25nm, 20nm, 11nm and 4nm. Upon retrieval of the effective material parameters, that exhibit negligible spatial dispersion similarly to the 20nm Ag/SiO₂ MMs treated in Sections III-IV, we present below the relative deviation of the ordinary and extraordinary permittivity of the effective

medium theory from our results: $\Delta\epsilon_{o_rel} = \frac{\epsilon_o - \epsilon_{o_EMT}}{\epsilon_o} \cdot 100\%$ and $\Delta\epsilon_{e_rel} = \frac{\epsilon_e - \epsilon_{e_EMT}}{\epsilon_e} \cdot 100\%$

respectively.

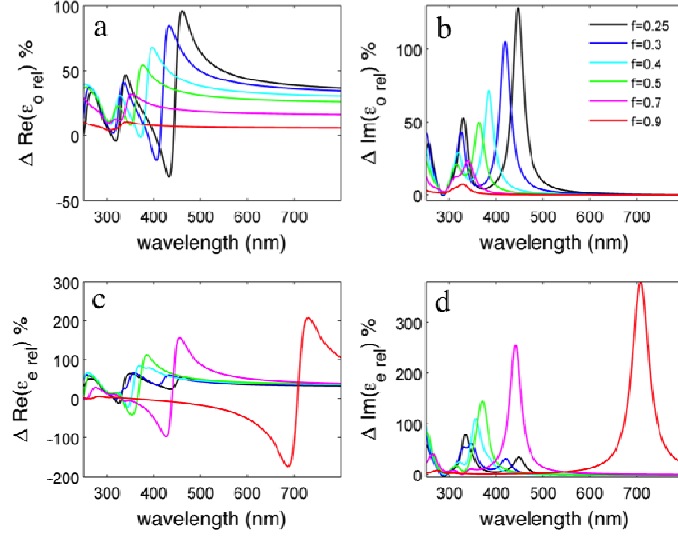


Fig. 8: relative difference $\Delta\epsilon_{o_rel}$ and $\Delta\epsilon_{e_rel}$ between exact results and effective medium theory results for Ag/SiO₂ multilayers of total thickness 140nm and 7 layers for different metallic filling fractions

Regarding the relative deviation of the ordinary permittivity (Fig. 8a, b), it decreases as the wavelength increases and the homogenization approximation becomes more valid. In the ordinary direction, the metallic character of individual Ag layers dominates over the collective response of the MM. Thus we observe better agreement between the exact results for ordinary permittivity and the effective medium results for increasing metallic filling fractions. However even for a Ag thickness of 32nm, which corresponds to a filling fraction of 0.9, the relative deviation of the effective medium theory results from our calculations is as high as 5.7%. The significant disagreement between the effective medium results and our calculations for wavelengths 400nm-500nm, especially for small filling fractions, originates from the difference at the ENZ wavelength of the ordinary permittivities between the effective medium picture and our method. Interband transitions in the permittivity of Ag lead to additional small amplitude Lorentzian-shaped features in the ordinary permittivity of MMs, according to our method. The interband transitions features are not as well preserved in the effective medium picture. Thus, it is these interband transitions that give rise to the smaller peaks for wavelengths in the 300nm-400nm range in Figs. 8a, and 8b.

In the extraordinary direction, the situation is reversed. Specifically, increasing metallic filling fractions give rise to stronger disagreement between the retrieved extraordinary permittivity and the effective medium result. The pole of ϵ_e is drastically affected by the filling fraction and redshifts as the filling fraction increases. As analyzed in Section IV, the pole of ϵ_e plays a significant role in the distinction between the elliptical and hyperbolic spectral regions supported by the HMMs. It contributes to an omnidirectional bandgap as demonstrated in Fig. 7 for a filling fraction of 0.5. Below we present the real parts of the denominators of Eq. (2b) for the electrically extraordinary wave, for the filling fractions considered in this section.

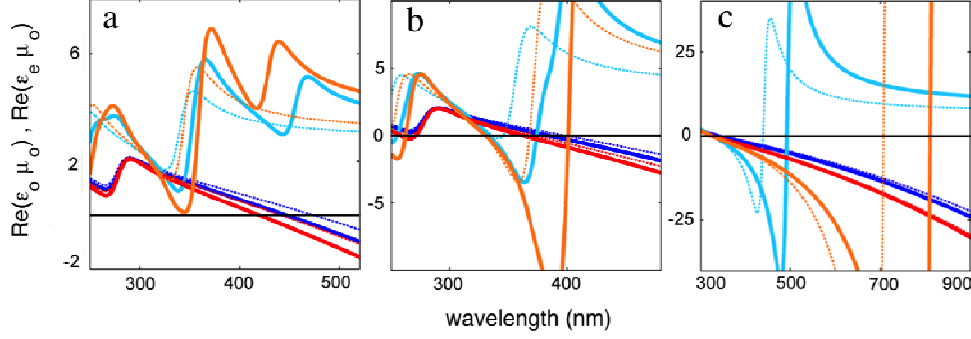


Fig. 9: real parts of $\mathcal{E}_o \mu_o$ and $\mathcal{E}_e \mu_o$. Blue solid lines- $\text{Re}(\mathcal{E}_o \mu_o)$ for a) $f=0.25$, b) $f=0.4$, c) $f=0.7$. Blue dotted lines- $\text{Re}(\mathcal{E}_o)$ in the effective medium limit for a) $f=0.25$, b) $f=0.4$, c) $f=0.7$. Light blue solid lines- $\text{Re}(\mathcal{E}_e \mu_o)$ for a) $f=0.25$, b) $f=0.4$, c) $f=0.7$. Light blue dotted lines- $\text{Re}(\mathcal{E}_e)$ in the effective medium limit for a) $f=0.25$, b) $f=0.4$, c) $f=0.7$. Red solid lines- $\text{Re}(\mathcal{E}_o \mu_o)$ for a) $f=0.3$, b) $f=0.5$, c) $f=0.9$. Red dotted lines- $\text{Re}(\mathcal{E}_o)$ in the effective medium limit for a) $f=0.3$, b) $f=0.5$, c) $f=0.9$. Orange solid lines- $\text{Re}(\mathcal{E}_e \mu_o)$ for a) $f=0.3$, b) $f=0.5$, c) $f=0.9$. Orange dotted lines- $\text{Re}(\mathcal{E}_e)$ in the effective medium limit for a) $f=0.3$, b) $f=0.5$, c) $f=0.9$.

For small filling fractions, neither our method nor effective medium theory yields a bandgap in the density of optical states, as shown in Fig. 9a. According to both our calculations and the effective medium results, the denominators $\mathcal{E}_o \mu_o$ and $\mathcal{E}_e \mu_o$ remain positive for small wavelengths, and in the longer wavelength regime we observe the hyperbolic type II dispersion due to the metallic character of \mathcal{E}_o . For a filling fraction of 0.4 in Fig. 9b, effective medium theory does not predict a hyperbolic type I region since $\text{Re}(\mathcal{E}_e)$ remains positive – see light blue dotted line. However according to our results such a region exists for wavelengths 334nm-374nm, because $\mathcal{E}_e \mu_o$ takes negative values-see solid light blue line in Fig. 9b. For a filling fraction of 0.5, the disagreement between the effective medium picture and our results is even stronger. Specifically, we observe an omnidirectional bandgap for wavelengths between 360nm-400nm where $\mathcal{E}_e \mu_o$ is negative simultaneously with $\mathcal{E}_o \mu_o$ -see orange and red solid lines respectively in Fig. 9b. Such a bandgap is not present according to effective medium theory- see orange and red dotted lines. For even higher filling fractions, in Fig. 9c, it is clear that the disagreement in the calculation of \mathcal{E}_e between our method and effective medium theory gives rise to spectral regions of different hyperbolicity types. For example, at a filling fraction $f=0.8$, our method predicts a bandgap in the density of optical states that extends to wavelengths 340-493nm, whereas in the effective medium limit the bandgap is significantly narrowed to the wavelength range 343nm-438nm.

In conclusion, by varying the total thickness and number of alternating metal and dielectric layers in Sections III and IV and by varying the individual layer thicknesses in this section, we find that the results of our method for the ordinary permittivity are less sensitive to both the total thickness and metallic filling fraction and in better agreement with the effective medium theory, than the extraordinary parameters, which are strongly dependent on the parameters discussed here. The extraordinary permittivity given by the effective medium theory has yielded poles positioned at wavelengths that are 30nm-100nm away from the poles predicted by our method for filling fractions ranging from 0.5 to 0.9.

VI. Conclusion

We present a method for determination of material parameters of uniaxial metamaterials. The method can retrieve the complex elements of the permittivity and permeability tensors for metamaterial with uniaxial anisotropy. The retrieved parameters are proved to be angle-independent, and thus constitute true material parameters with negligible angular dispersion in the long wavelength limit. We studied theoretically the effect of a finite number of layers in planar metal/dielectric metamaterials on their effective parameters, and compared the results to effective medium theory and Bloch theory. We also considered the effects of individual layer thicknesses and metallic filling fraction on the effective parameters and compared to the effective medium results. Importantly, we found a strong diamagnetic character for those HMMs in the optical regime. We note that this physically realistic and accurate analytical retrieval method improves upon existing effective medium approximations for the isofrequency surfaces of HMMs, as evidenced by the existence of an effective gap in the photonic density of states for electrically extraordinary waves, which is not predicted by the effective medium theory for MMs with low metallic filling fractions and finite total thickness. Our method is general and can be applied to any MM with uniaxial anisotropy: once the forward problem is solved and the scattering parameters are determined, the parameter retrieval algorithm can be directly applied. For example, it can be applied to nanowire HMMs (a finite elements method is required in this case for the solution of the forward problem). Notably, our method provides the means for the investigation of a magnetic HMM with magnetic topological transitions in the optical regime, similar to the recent work in the microwave regime¹².

Acknowledgments

We acknowledge fruitful discussions with Prof. E. N. Economou and Dr. Krishnan Thyagarajan. This work was supported by the Multidisciplinary University Research Initiative Grant (Air Force Office of Scientific Research MURI, FA9550-12-1-0488). G. Papadakis acknowledges support by a National Science Foundation Graduate Research Fellowship.

Author Information

Corresponding author email: gpapadak@caltech.edu

Notes: The authors declare no competing financial interest

Appendix

A. Homogenization

We present below the equation used for determining the normal component of the wave vector k_z in a MM slab that we refer to in Eq. (2a) and (2b), which is work by C. Menzel et al. in [13]. The equation is obtained by solving the analytical expressions for transmission and reflection coefficients t and r respectively from a homogeneous isotropic slab of total thickness d embedded between media ‘c’ referring to cladding and ‘s’ referring to substrate in terms of k_z .

$$k_z = \pm \frac{1}{d} \arccos \left\{ \frac{k_s(1-r^2) + k_c(t/A)^2}{(t/A)(k_s(1-r) + k_c(1+r))} \right\} + 2m\pi \quad (\text{A. 1})$$

where $m \in \mathbb{Z}$. The equation is valid for TE and TM polarization, with the A being: $A=1$ for TE polarization and $A = \sqrt{\epsilon_s \mu_c / \epsilon_c \mu_s}$ for TM polarization, where $\epsilon_c, \mu_c, \epsilon_s, \mu_s$ being the electric permittivity and magnetic permeability of the cladding and substrate layers respectively. k_c is given by

$$k_c = \sqrt{\frac{\epsilon_c}{\mu_c}} \frac{\omega}{c} \sin \theta_{in} \text{ for TE polarization and } k_c = \sqrt{\frac{\mu_c}{\epsilon_c}} \frac{\omega}{c} \sin \theta_{in} \text{ for TM polarization. Similarly,}$$

$$k_s = \sqrt{\frac{\epsilon_s}{\mu_s}} \frac{\omega}{c} \sin \theta_{out} \text{ for TE polarization and } k_s = \sqrt{\frac{\mu_s}{\epsilon_s}} \frac{\omega}{c} \sin \theta_{out} \text{ for TM polarization. Here, } \theta_{in} \text{ and } \theta_{out}$$

refer to the angles shown in Fig. 1d and $\sqrt{\epsilon_c \mu_c} \sin \theta_{in} = \sqrt{\epsilon_s \mu_s} \sin \theta_{out}$. The value of m is chosen such that k_z is a continuous function of the wavelength. The sign in Eq. (A.1) is chosen such that the passivity conditions are satisfied, in other works, the imaginary part of k_z must be positive. For determination of the wave parameters ϵ_{TE} , μ_{TE} , ϵ_{TM} and μ_{TM} , a generalized impedance ξ is utilized.

$$\xi = \pm \sqrt{\frac{k_s^2 (r-1)^2 - k_c^2 (t/A)^2}{(r+1)^2 - (t/A)^2}} \quad (\text{A. 2})$$

The real part of the impedance should remain positive for a passive medium. Then $\mu_{TE/TM} = k_z / \xi$. The parameters ϵ_{TE} and ϵ_{TM} can be determined through the dispersion equation for an isotropic material:

$$\frac{\omega^2}{c^2} \epsilon_{TE/TM}(k_x, \omega) = \frac{k_x^2 + k_z^2}{\mu_{TE/TM}} \quad (\text{A. 3})$$

We note that we have interchanged the parameters ϵ_{TM} and μ_{TM} , with respect to [13] to be consistent with the notation in the main text and supplemental information. Here $k_x = \sqrt{\epsilon_c \mu_c} \sin \theta_{in}$ is the in-plane wave

vector, which is conserved above, inside and below the MM slab. The modal effective refractive indices for TE and TM polarizations are: $n_{TE} = \sqrt{\epsilon_{TE}\mu_{TE}}$ and $n_{TM} = \sqrt{\epsilon_{TM}\mu_{TM}}$ respectively.

B. The effective permeability of Ag/SiO₂ HMMs and conservation of energy

Regarding the negative imaginary part of μ_o and μ_e for MMs consisting of more than 5 alternating layers of Ag and SiO₂ (see Fig. 3c, d and Fig. 5b), we assure that conservation of energy is not violated because¹:

1. Through the homogenization¹³, a positive imaginary part of k_z was imposed. The parameters μ_o and μ_e are calculated through k_z (through Eq. (2a) and (2b)), thus assuring a passive medium.
2. The modal effective index of the TE and TM mode are $n_{TE} = \sqrt{\epsilon_{TE}\mu_{TE}}$ and $n_{TM} = \sqrt{\epsilon_{TM}\mu_{TM}}$ respectively. The imaginary parts of both n_{TE} and n_{TM} are positive as shown below for the 7 layer Ag/SiO₂ MM, also assuring a passive medium.

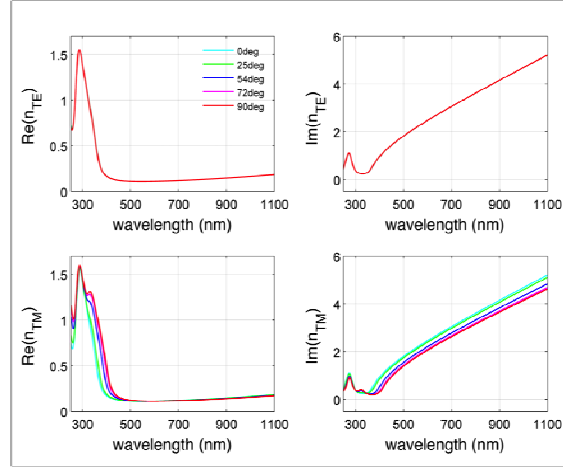


Fig. 10: Angle dependence of n_{TE} and n_{TM} for 7 layer Ag/SiO₂ MM

Thus, the negative imaginary part of μ_o in Fig. 3c and of μ_e in Fig. 3d is not a violation of conservation of energy but rather a consequence of the diamagnetic response of our MMs for parameters obeying Kramers-Kronig relations (See [36] and references therein). We obtain similar results for the 3, 5, 15, 17, 27 layer MMs considered in Fig. 5, and the imaginary parts of the modal indices n_{TE} and n_{TM} for both polarizations remain positive for all incident angles.

3. Another way to verify that the retrieved permeability tensors do not violate conservation of energy is to calculate the absorption for both polarizations from the MM slab. The results are shown below for the 7 layer MM. Absorption, along with transmittance and reflectance for both polarizations has been calculated not only using the transfer matrix²⁸ method applied to the multilayer MMs (forward problem) but also to the equivalent effective single homogeneous slabs with the retrieved effective parameters

¹ An extended discussion in the literature³⁶ V. A. Markel, Physical Review E **78**, 026608 (2008). regarding the issue of the negative imaginary part of the permeability of a diamagnetic MM is in agreement with our results.

(inverse problem).

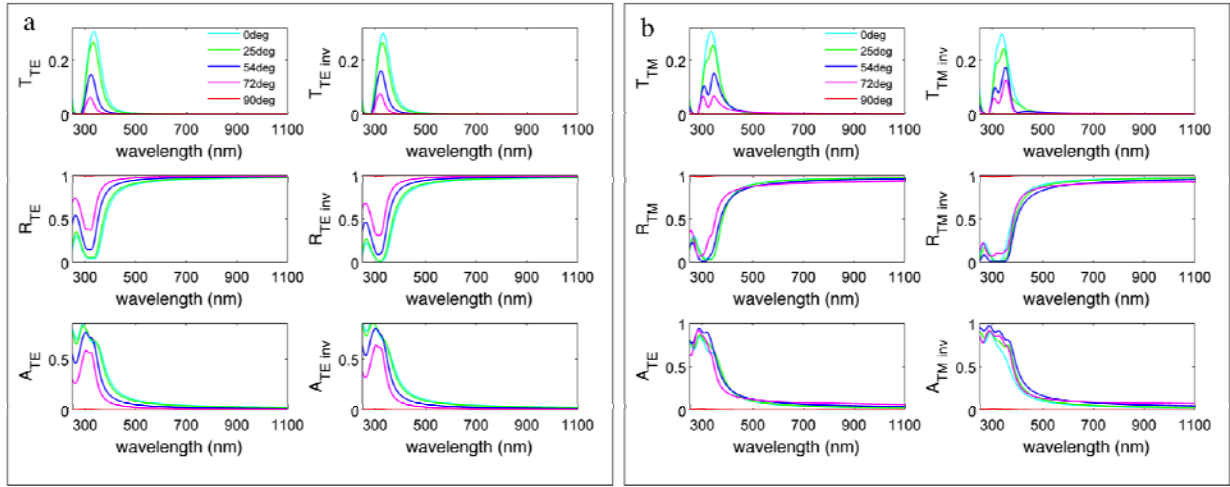


Fig. 11: Sum of transmittance and reflectance for TE and TM polarization: $T_{TE}, R_{TE}, T_{TM}, R_{TM}$ stand for calculated transmittance and reflectance from the 7 layer MM structure using the transfer matrix. $T_{TEinv}, R_{TEinv}, T_{TMinv}, R_{TMinv}$ stand for calculated transmittance and reflectance from a single effective layer with index n_{TE} and n_{TM} shown in Fig. 10

The absorption coefficient, presented in Fig. 11, remains smaller than unity in both cases, assuring conservation of energy.

It is also worth noting the similarity between the scattering parameters (transmittance, reflectance and absorption) of the forward and inverse scattering problem both for TE and TM polarization, which demonstrates the accuracy of the retrieval procedure: the forward problem of calculating the reflection and transmission from the multilayer structure is equivalent to the inverse problem of calculating the transmission and reflection from an effective slab with the retrieved parameters. We obtain similar results with very good agreement between the forward and inverse problem for all the considered number of layer MMs shown in Fig.4 and 5.

References

- 1 D. R. Smith, W. J. Padilla, D. C. Vier, S. C. Nemat-Nasser, and S. Schultz, *Physical Review Letters* **84**, 4184 (2000).
- 2 V. G. Veselago, *Soviet Physics Uspekhi* **10** (1964).
- 3 R. Maas, J. Parsons, N. Engheta, and A. Polman, *Nat Photon* **7**, 907 (2013).
- 4 N. Engheta, *Science* **340**, 286 (2013).
- 5 J. B. Pendry, *Physical Review Letters* **85**, 3966 (2000).
- 6 R. W. Ziolkowski and N. Engheta, in *Metamaterials* (John Wiley & Sons, Inc., 2006), p. 1.
- 7 A. Poddubny, I. Iorsh, P. Belov, and Y. Kivshar, *Nat Photon* **7**, 948 (2013).
- 8 J. Yao, Z. Liu, Y. Liu, Y. Wang, C. Sun, G. Bartal, A. M. Stacy, and X. Zhang, *Science* **321**, 930 (2008).
- 9 Z. Liu, H. Lee, Y. Xiong, C. Sun, and X. Zhang, *Science* **315**, 1686 (2007).
- 10 Z. Jacob, J.-Y. Kim, G. Naik, A. Boltasseva, E. Narimanov, and V. Shalaev, *Appl. Phys. B* **100**, 215 (2010).
- 11 H. N. S. Krishnamoorthy, Z. Jacob, E. Narimanov, I. Kretzschmar, and V. M. Menon, *Science* **336**, 205 (2012).
- 12 A. V. Shchelokova, D. S. Filonov, P. V. Kapitanova, and P. A. Belov, *Physical Review B* **90**, 115155 (2014).
- 13 C. Menzel, C. Rockstuhl, T. Paul, F. Lederer, and T. Pertsch, *Physical Review B* **77**, 195328 (2008).
- 14 D. R. Smith, S. Schultz, P. Markoš, and C. M. Soukoulis, *Physical Review B* **65**, 195104 (2002).
- 15 X. Chen, T. M. Grzegorzczak, B.-I. Wu, J. Pacheco, and J. A. Kong, *Physical Review E* **70**, 016608 (2004).
- 16 Y. Minowa, T. Fujii, M. Nagai, T. Ochiai, K. Sakoda, K. Hirao, and K. Tanaka, *Opt. Express* **16**, 4785 (2008).
- 17 D. R. Smith, D. C. Vier, T. Koschny, and C. M. Soukoulis, *Physical Review E* **71**, 036617 (2005).
- 18 C. Menzel, T. Paul, C. Rockstuhl, T. Pertsch, S. Tretyakov, and F. Lederer, *Physical Review B* **81**, 035320 (2010).
- 19 A. Andryieuski, C. Menzel, C. Rockstuhl, R. Malureanu, F. Lederer, and A. Lavrinenko, *Physical Review B* **82**, 235107 (2010).
- 20 A. V. Chebykin, A. A. Orlov, C. R. Simovski, Y. S. Kivshar, and P. A. Belov, *Physical Review B* **86**, 115420 (2012).
- 21 A. V. Chebykin, A. A. Orlov, A. V. Vozianova, S. I. Maslovski, Y. S. Kivshar, and P. A. Belov, *Physical Review B* **84**, 115438 (2011).
- 22 V. P. Drachev, V. A. Podolskiy, and A. V. Kildishev, *Opt. Express* **21**, 15048 (2013).
- 23 C. L. Cortes, W. Newman, S. Molesky, and Z. Jacob, *Journal of Optics* **14**, 063001 (2012).
- 24 Y. Guo and Z. Jacob, *Opt. Express* **21**, 15014 (2013).
- 25 C. L. Cortes and Z. Jacob, *Physical Review B* **88**, 045407 (2013).
- 26 A. Fang, T. Koschny, and C. M. Soukoulis, *Physical Review B* **79**, 245127 (2009).

- 27 X. Chen, B.-I. Wu, J. A. Kong, and T. M. Grzegorzcyk, *Physical Review E* **71**, 046610 (2005).
- 28 P. Yeh, *Optical waves in layered media* (John Wiley & Sons, Hoboken, New Jersey, 1988).
- 29 V. Agranovich and V. Kravtsov, *Solid State Communications* **55**, 85 (1985).
- 30 D. E. Aspnes, *American Journal of Physics* **50**, 704 (1982).
- 31 Y. Liu, G. Bartal, and X. Zhang, *Opt. Express* **16**, 15439 (2008).
- 32 S. Foteinopoulou, M. Kafesaki, E. N. Economou, and C. M. Soukoulis, *Physical Review B* **84**, 035128 (2011).
- 33 J. Kim, V. P. Drachev, Z. Jacob, G. V. Naik, A. Boltasseva, E. E. Narimanov, and V. M. Shalaev, *Opt. Express* **20**, 8100 (2012).
- 34 K. S. Potter and J. H. Simmons, *Optical Materials* (Academic Press, 2000)
- 35 J. D. Joannopoulos, S. G. Johnson, J. N. Winn, and R. D. Meade, *Photonic Crystals: Molding the Flow of Light* (Princeton University Press, 2008).
- 36 V. A. Markel, *Physical Review E* **78**, 026608 (2008).